A Controllable Membrane-Type Humidifier for Fuel Cell Applications—Part II: Controller Design, Analysis and Implementation

Denise A. McKay[1]
Picker Engineering Program,
Smith College,
Northampton, MA 01063
e-mail: dmckay@smith.edu

Anna G. Stefanopoulou
Fellow ASME

Jeffrey Cook

Fuel Cell Control Laboratory,
University of Michigan,
Ann Arbor, MI 48109

A membrane-based gas humidification apparatus was employed to actively manage the amount of water vapor entrained in the reactant gas supplied to a fuel cell stack. The humidification system utilizes a gas bypass and a series of heaters to achieve accurate and fast humidity and temperature control. A change in fuel cell load induces a reactant mass flow rate disturbance to this humidification system. If not well regulated, this disturbance creates undesirable condensation and evaporation dynamics, both to the humidification system and the fuel cell stack. Therefore, controllers were devised, tuned, and employed for temperature reference tracking and disturbance rejection. Two heater controller types were explored: on-off (thermostatic) and variable (proportional integral), to examine the ability of the feedback system to achieve the control objectives with minimal hardware and software complexities. The coordination of the heaters and the bypass valve is challenging during fast transients due to the different time scales, the actuator constraints, and the sensor responsiveness. [DOI: 10.1115/1.4001020]

1 Introduction

For the advancement of polymer electrolyte membrane fuel cell (PEMFC) systems, achieving adequate thermal and humidity regulation remains a critical hurdle [1]. To maintain high membrane conductivity and durability, the supplied reactants require humidification. However, excess water can condense and affect fuel cell performance [2], requiring accurate and fast control of the gas humidity supplied to the fuel cell [3].

Several humidification strategies were considered for fuel cell reactant pretreatment, including bubblers or spargers [4], and passive membrane-based humidifiers integral to the PEMFC stack [2,5,6]. For active humidity and temperature control of the reactants supplied to a PEMFC stack, a stand-alone membrane-based humidification system was designed and experimentally validated in Part I of this work [7]. The humidification apparatus decouples the passive membrane humidifier from the PEMFC cooling loops with the addition of an external gas bypass and a separate water circulation system (PEMFC reactant exhaust streams could also be used), to provide a controllable reactant relative humidity at a regulated temperature. This humidification system apparatus is conceptually similar to that proposed by Wheat et al. [8]. The operation of the humidifier consists of a dry reactant gas and liquid water delivered to opposite sides of a membrane humidifier to produce a saturated gas. Another stream of dry reactant gas bypasses the humidifier. The combination of the saturated and dry gas streams produces a reactant-vapor mixture at a desired relative humidity. A diagram of the humidification system is provided in Fig. 1.

The humidification system control strategy in Ref. [8] relied on a relative humidity sensor for feedback control of an electronic bypass valve, due to the strong coupling between gas humidity and temperature. However, thermal regulation must also be considered. In developing our control strategy, critical steps were accomplished by properly selecting the controller references used for temperature feedback; employing a static feedforward mapping for humidity control to eliminate the need for an expensive and slow relative humidity probe for feedback control; and providing a thorough comparison of the use of on/off versus variable gas heaters in achieving thermal regulation.

Controllers were designed and a reproducible methodology for controller tuning is presented to coordinate the three resistive heaters, as well as the mass fractional split of air flow between the humidifier and the air bypass. These controllers must regulate the temperature of the dry air leaving the bypass, and join the saturated air leaving the humidifier. Should the temperatures of these two gas streams not be well regulated during air mass flow disturbances due to the fuel cell system load demand, condensation or dehydration will occur. Similar problems arise in engine thermal management systems, employing either a valve or servo motor to bypass the coolant around the heat exchanger [9,10]. The coordination of the heaters and the bypass valve is challenging during fast transients due to the different time scales, the actuator constraints, and the sensor responsiveness.

2 Hardware and System Overview

The humidification system hardware, designed in collaboration with the Schatz Energy Research Center at Humboldt State University, was installed in the Fuel Cell Control Laboratory at the University of Michigan. A detailed description of the system actuators and sensors was provided in Part I of this work [7]. The system was designed to deliver moist air at 45°C–65°C and 50–100% relative humidity at dry air mass flow rates up to 40 slm, corresponding to 300% excess oxygen in the cathode of a 0.5 kW fuel cell. The humidifier system consists of five control volumes, namely, the water heater, humidifier, reservoir, bypass, and mixer. Figure 1 shows the interaction of the air and liquid water as they move through these control volumes.

[1]Corresponding author.

Contributed by the Advanced Energy Systems Division of ASME for publication in the JOURNAL OF FUEL CELL SCIENCE AND TECHNOLOGY. Manuscript received September 29, 2009; final manuscript received November 17, 2009; published online November 1, 2010. Review conducted by Nigel M. Sammes.

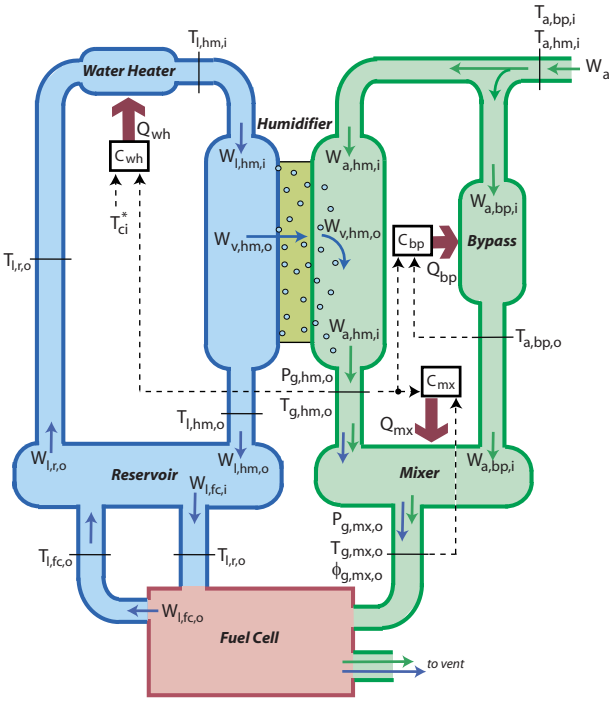

Fig. 1 Overview of the control architecture for the external humidification system. Dashed lines indicate input temperatures to the controller *C*.

When the humidification system is coupled with a fuel cell, the total dry air mass flow through the system W_a depends on the amount of current produced by the fuel cell and can be thought of as a system disturbance. The fraction of air supplied to the bypass r_{bp} or humidifier r_{hm} is controlled with mass flow controllers that regulate the bypass and humidifier air mass flow rates $W_{a,\text{bp},i}$ and $W_{a,\text{hm},i}$. The humidifier produces a saturated air stream at a temperature $T_{g,\text{hm},o}$ dependent upon the supplied liquid water temperature $T_{l,\text{hm},i}$. Air bypassing the humidifier is heated with a 50 W heater Q_{bp}. The saturated air stream from the humidifier and dry air stream from the bypass are combined in the mixer to produce a desired air-vapor mixture relative humidity $\phi_{g,\text{mx},o}$ to be supplied to the fuel cell. A 52 W resistive heater Q_{mx} is used in the mixer for temperature control and to minimize condensation during the mixing of the saturated and dry gases.

Liquid water is circulated from the reservoir through the water heater and humidifier using a pump and manual throttle valve for controlling the liquid water flow rate. The water reservoir is shared with the fuel cell coolant loop, containing a heat exchanger, fan, and circulation pump, which are not shown. Liquid water from the fuel cell is an input to the reservoir at the fuel cell coolant temperature $T_{l,\text{fc},o}$. To mitigate reservoir thermal disturbances and offset heat losses to the ambient, a 1000 W resistive heater Q_{wh} is used to heat the liquid water before entering the humidifier.

A data acquisition and signal conditioning subsystem, along with control and monitoring software, was utilized to coordinate the humidification system. Software coded in LABVIEW® was employed on a standard desktop PC computer. This computer is equipped with PCI data acquisition cards connected through the signal conditioning system to the instruments. The signal scan rate is approximately 10 Hz, with 4 Hz low-pass filters on the analog signals, and the data file is updated at a rate of 2 Hz. Finally, the digital inputs and outputs are processed through an Opto-22 digital backplane with optically isolated solid state relays. The AC heater actuators are controlled by either turning these digital relays on and off (in the case of thermostatic control), or by providing a continuous signal to a phase-fired solid state relay that controls the fraction of a 60 Hz sine wave to the heater that corresponds to the desired heater power (in the case of variable proportional integral control).

3 Modeling Summary

This section summarizes the humidification system modeling effort that was experimentally validated in Part I of this work [7]. Applying the conservation of mass and energy, the resulting state equations are expressed for the bypass as

$$\frac{dT_{a,\text{bp}}}{dt} = \frac{1}{m_{\text{bp}}C_{\text{bp}}}[Q_{\text{bp}} + W_{a,\text{bp},i}C_{p,a}(T_{a,\text{bp},i} - T_{a,\text{bp},o}) - \hbar_{b2\text{amb,bp}}A_{b2\text{amb,bp}}(T_{a,\text{bp}} - T_{\text{amb}})] \quad (1)$$

the water reservoir

$$\frac{dT_{l,r}}{dt} = \frac{1}{m_{l,r}C_{l,r}}[W_{l,\text{fc},i}C_{p,l}(T_{l,\text{fc},o} - T_{l,r,o}) + W_{l,\text{wh},i}C_{p,l}(T_{l,\text{hm},o} - T_{l,r,o}) - \hbar_{l2b,r}A_{l2b,r}(T_{l,r} - T_{b,r})] \quad (2a)$$

$$\frac{dT_{b,r}}{dt} = \frac{1}{m_{b,r}C_{b,r}}[\hbar_{l2b,r}A_{l2b,r}(T_{l,r} - T_{b,r}) - \hbar_{b2\text{amb},r}A_{b2\text{amb},r}(T_{b,r} - T_{\text{amb}})] \quad (2b)$$

the water heater

$$\frac{dT_{l,\text{wh}}}{dt} = \frac{1}{m_{l,\text{wh}}C_{l,\text{wh}}}[W_{l,\text{hm},i}C_{p,l}(T_{l,r,o} - T_{l,\text{hm},i}) + \hbar_{b2l,\text{wh}}A_{b2l,\text{wh}}(T_{b,\text{wh}} - T_{l,\text{wh}})] \quad (3a)$$

$$\frac{dT_{b,\text{wh}}}{dt} = \frac{1}{m_{b,\text{wh}}C_{b,\text{wh}}}[Q_{\text{wh}} - \hbar_{b2l,\text{wh}}A_{b2l,\text{wh}}(T_{b,\text{wh}} - T_{l,\text{wh}}) - \hbar_{b2\text{amb,wh}}A_{b2\text{amb,wh}}(T_{b,\text{wh}} - T_{\text{amb}})] \quad (3b)$$

the humidifier

$$\frac{dT_{l,\text{hm}}}{dt} = \frac{1}{m_{l,\text{hm}}C_{l,\text{hm}}}[W_{l,\text{hm},i}C_{p,l}(T_{l,\text{hm},i} - T_{l,\text{hm},o}) - W_{v,\text{hm},o}(h_{g,\text{hm},o} - C_{p,l}T_{l,\text{hm},o}) - \hbar_{l2g,\text{hm}}A_{l2g,\text{hm}}(T_{l,\text{hm}} - T_{g,\text{hm}}) - \hbar_{l2\text{amb,hm}}A_{l2\text{amb,hm}}(T_{l,\text{hm}} - T_{\text{amb}})] \quad (4a)$$

$$\frac{dT_{g,\text{hm}}}{dt} = \frac{1}{m_{g,\text{hm}}C_{g,\text{hm}}}[W_{a,\text{hm},i}C_{p,a}(T_{g,\text{hm},i} - T_{g,\text{hm},o}) + \hbar_{l2g,\text{hm}}A_{l2g,\text{hm}}(T_{l,\text{hm}} - T_{g,\text{hm}})] \quad (4b)$$

and the mixer

$$\frac{dT_{g,\text{mx}}}{dt} = \frac{1}{m_{g,\text{mx}}C_{g,\text{mx}}}[W_{a,\text{bp},i}C_{p,a}(T_{a,\text{bp},o} - T_{g,\text{mx},o}) + (W_{a,\text{hm},i}C_{p,a} + W_{v,\text{hm},o}C_{p,v})(T_{g,\text{hm},o} - T_{g,\text{mx},o}) + \hbar_{b2g,\text{mx}}A_{b2g,\text{mx}}(T_{b,\text{mx}} - T_{g,\text{mx}})] \quad (5a)$$

$$\frac{dT_{b,\text{mx}}}{dt} = \frac{1}{m_{b,\text{mx}}C_{b,\text{mx}}}[Q_{\text{mx}} - \hbar_{b2g,\text{mx}}A_{b2g,\text{mx}}(T_{b,\text{mx}} - T_{g,\text{mx}}) - \hbar_{b2\text{amb,mx}}A_{b2\text{amb,mx}}(T_{b,\text{mx}} - T_{\text{amb}})] \quad (5b)$$

The system parameters were determined either from established published literature, taken from measurements of the physical hardware, or experimentally identified, as described in Part I of this work [7], and are reproduced here in Table 1. Due to the inability to measure the internal temperature states, approximations were employed to relate the internal states to the measurable outlet temperatures, and are summarized by

$$T_{a,\text{bp},o} = 2T_{\text{bp}} - T_{a,\text{bp},i} \quad (6a)$$

Table 1 Model parameters

Mass (g)	Specific heat (J/kg K)	Area (m^2)	Heat transfer (W/m^2 K)
$m_{bp}=80$	$C_{bp}=460$	$A_{bp}=0.012$	$\hbar_{bp}=10.8-21822W_{a,bp,i}$
$m_{l,wh}=50$	$C_{l,wh}=4180$	$A_{b2l,wh}=0.020$	$\hbar_{b2l,wh}=139.8$
$m_{b,wh}=780$	$C_{b,wh}=460$	$A_{wh}=0.028$	$\hbar_{b2amb,wh}=0$
$m_{l,hm}=240$	$C_{l,hm}=4180$	$A_{l2amb,hm}=0.202$	$\hbar_{l2amb,hm}=22.5$
$m_{a,hm}=18$	$C_{a,hm}=983$	$A_{l2a,hm}=0.03$	$\hbar_{l2a,hm}=41029W_{a,hm,i}^{0.95}$
$m_{g,mx}=10$	$C_{g,mx}=863$	$A_{b2g,mx}=0.009$	$\hbar_{b2g,mx}=2819W_{a}^{0.54}$
$m_{b,mx}=745$	$C_{b,mx}=460$	$A_{mx}=0.012$	$\hbar_{b2amb,mx}=25.8$
$m_{l,r}=2800$	$C_{l,r}=4180$	$A_{l2b,r}=0.075$	$\hbar_{l2b,r}=167.5$
$m_{b,r}=1540$	$C_{b,r}=957$	$A_{b2amb,r}=0.087$	$\hbar_{b2amb,r}=80.0$
	$C_{p,a}=1004$		
	$C_{p,v}=1872$		
	$C_{p,l}=4180$		

$$T_{l,\mathrm{wh},o} = 2T_{l,\mathrm{wh}} - T_{l,r,o} \tag{6b}$$

$$T_{l,\mathrm{hm},o} = 2T_{l,\mathrm{hm}} - T_{l,\mathrm{hm},i} \tag{6c}$$

$$T_{l,r,o} = T_{l,r} \tag{6d}$$

$$T_{a,\mathrm{hm},o} = 2T_{a,\mathrm{hm}} - T_{a,\mathrm{hm},i} \tag{6e}$$

$$T_{g,\mathrm{mx}} = T_{g,\mathrm{mx},o} \tag{6f}$$

Finally, the relative humidity of the mixer outlet gas is estimated by

$$\phi_{g,\mathrm{mx},o} = \phi_{g,\mathrm{hm},o} r_{\mathrm{hm}} \frac{p_{g,\mathrm{hm},o}^{\mathrm{sat}}}{p_{g,\mathrm{mx},o}^{\mathrm{sat}}} \left(\frac{p_{g,\mathrm{mx},o}}{p_{g,\mathrm{hm},o} - r_{\mathrm{bp}} \phi_{g,\mathrm{hm},o} p_{g,\mathrm{hm},o}^{\mathrm{sat}}} \right) \tag{7}$$

The locations of the measurements and disturbances are shown in Fig. 1. The inputs to the system are heater power Q and the mass fraction of air diverted through the bypass r_{bp}; the states are the respective temperatures T; the disturbances are the total dry air mass flow rate W_a, the air temperature supplied to the system $T_{a,\mathrm{hm},i}$ and $T_{a,\mathrm{bp},i}$, and the ambient temperature T_{amb}; and the system output is the air relative humidity leaving the mixer $\phi_{g,\mathrm{mx},o}$.

4 Controller System Architecture

With the model of the external humidification system presented in Sec. 3, controllers were designed and tuned to coordinate the three resistive heaters, as well as the fraction of air supplied to the humidifier and bypass. The three heaters must be well coordinated to regulate the system temperatures and mitigate the effect of disturbances.

An overview of the control architecture is provided in Fig. 2. An error signal is calculated (difference between the reference and actual temperatures) as an input to the heater controllers. The heaters are then controlled by determining a desired heater power for the respective control volumes given the error signal. The fractional split of dry air mass flow between the humidifier and the bypass is commanded using a static nonlinear feedforward map given a desired relative humidity and temperature at the cathode inlet (mixer outlet). This section introduces the nonlinear static feedforward mapping devised for air mass flow control, the reference temperatures used for thermal regulation, and the plant linearization performed in preparation for controller tuning.

4.1 Nonlinear Feedforward for Air Mass Flow Control. A nonlinear, physics based, feedforward mapping is used to control the amount of air supplied to the bypass and the humidifier to achieve the desired relatively humidity of the gases leaving the mixer and supplied to the cathode inlet of the PEMFC stack. This feedforward mapping is a function of both the measured and desired temperature states, relative humidity estimations, and total gas pressure measurements. The use of relative humidity feedback control would require either a water vapor mass flow rate or relative humidity measurement at the mixer outlet. In practice, both such measurements are prohibitively expensive, motivating the rationale for using feedforward and neglecting relative humidity feedback control. Although an observer based relative humidity feedback estimation could be employed, the coupling between humidity and temperature poses a performance tradeoff between these two control objectives.

To calculate the desired split of dry air mass flow between the humidifier and the bypass, mass conservation is applied. Assuming that in steady-state the mass flow rate of water vapor and air entering the mixer are equal to the mass flow rates leaving the mixer, and applying the definition for the humidity ratio ω

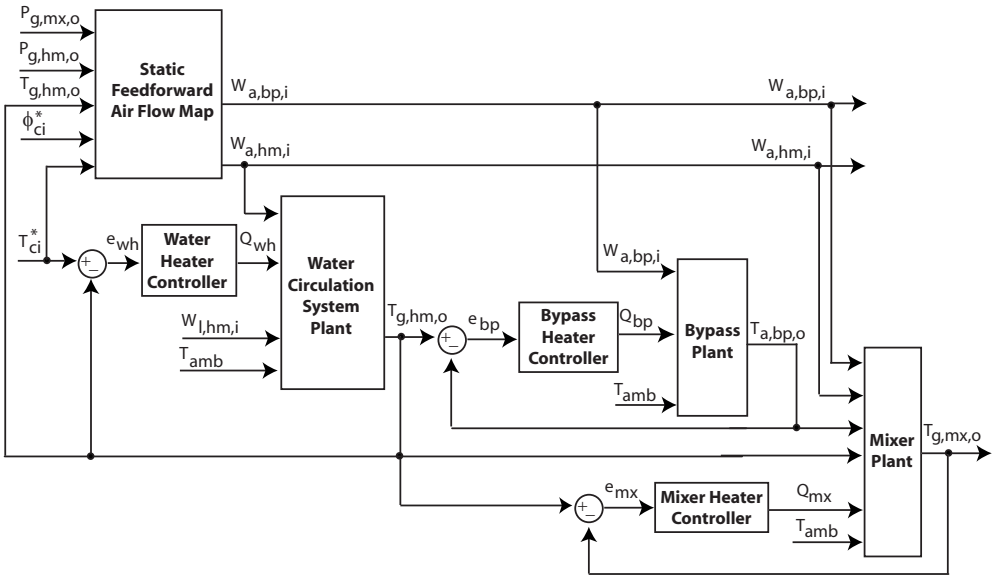

Fig. 2 Humidification system control architecture

$= M_v \phi p^{\text{sat}} / M_a (p - \phi p^{\text{sat}})$, the required fraction of air supplied to the humidifier $r_h = W_{a,\text{hm},i} / W_a$ can be expressed as

$$r_{\text{hm}} = \frac{\phi^*_{g,\text{mx},o} p^{\text{sat}*}_{g,\text{mx},o} (p_{g,\text{hm},o} - \phi_{g,\text{hm},o} p^{\text{sat}}_{g,\text{hm},o})}{\phi_{g,\text{hm},o} p^{\text{sat}}_{g,\text{hm},o} (p_{g,\text{mx},o} - \phi^*_{g,\text{mx},o} p^{\text{sat}*}_{g,\text{mx},o})} \tag{8}$$

where a superscript * has been used to denote the desired reference values. The commanded air mass flow rates through the humidifier and the bypass are

$$W_{a,\text{hm},i} = r_{\text{hm}} W_a \tag{9a}$$

$$W_{a,\text{bp},i} = W_a - W_{a,\text{hm},i} \tag{9b}$$

4.2 Reference Temperatures. To properly coordinate the heaters using feedback control, reference temperatures must be established for the mixer, bypass, and humidifier air outlets. The error, or difference between the reference and actual measured temperatures, $\delta e = \delta T^* - \delta T$, where δ indicates a deviation from nominal conditions, can then be formulated into control objectives for each of the heaters. It is important to note that these actual temperatures must be measured to implement direct (nonobserver based) feedback control.

Several reference temperature choices exist for thermal regulation of the humidification system, depending upon the response times of the bypass, mixer, and water circulation systems. These reference temperatures have drastically different implications with respect to controller performance. For example, if the water circulation, bypass, and mixer systems had similar response times, they could be independently coordinated, motivating the selection of the desired cathode inlet temperature as the reference temperature for all three systems.

It will be shown later in Sec. 4.3 that the intermediate step of heating liquid water to raise the humidifier gas temperature causes the slowest thermal response of the three systems. Because both the mixer and bypass systems are faster than the water circulation system, condensation or evaporation can be avoided upon gas mixing if both the mixer and the bypass track the temperature dynamics of the water circulation system. The resulting reference temperatures

$$T^*_{g,\text{mx},o} = T_{g,\text{hm},o}, \quad T^*_{g,\text{hm},o} = T^*_{\text{ca},i}, \quad T^*_{a,\text{bp},o} = T_{g,\text{hm},o} \tag{10}$$

will result in a slower system thermal response, but will maintain the desired relative humidity. Figure 1 shows the location of these reference temperatures with the measured states and respective control volumes clearly indicated. An important distinction is made here, the reference temperature for the water circulation system will be either constant or variable, depending upon the water management demands of the PEMFC stack. However, both the mixer and bypass reference temperatures are always variable and depend on the dynamics in the water circulation system, not the dynamics in the PEMFC stack.

This control strategy relies on the significant bandwidth separation observed between the slow closed loop water circulation system and the fast bypass and mixer systems, and should be reconsidered if the volumes were designed to be significantly different than those presented in this work. Additionally, if the desired cathode inlet temperature were deemed to be more critical to maintain than relative humidity, the mixer could track the desired cathode inlet temperature, implying that the mixer heater is controlled irrespective of the bypass and water circulation system conditions.

4.3 Plant Linearization. Due to the cascaded nature of the humidification system, the mixer and bypass control volumes can be analyzed separately from the water circulation system, allowing for independent controller design. The system of ordinary differential equations, shown in Sec. 3, was expressed analytically in state space, where the control volume outlet temperatures represented the states, the heater actuators represented the system inputs, the air mass flow rate represented the system disturbance, and the liquid water mass flow rate and ambient temperature were assumed to be constant.

Table 2 Nominal conditions used for system linearization

Variable	Nominal value
W^o_a	0.6 g/s
r^o_h	0.7
$T^o_{a,\text{hm},i} = T^o_{a,\text{bp},i}$	20°C
$W^o_{l,\text{hm},i}$	30 g/s
T^o_{amb}	27°C
$p^o_{g,\text{hm},o}$	102.57 kPa abs
$T^o_{a,\text{bp},o} = T^o_{g,\text{hm},o}$	55°C

Using this state space representation, the system was linearized about a set of nominal conditions, listed in Table 2. As previously discussed, the humidification system was designed to regulate the cathode air supplied to an eight-cell PEMFC stack with an active area of 300 cm^2. Applying a 0.3 A/cm^2 electric load to this PEMFC stack requires 0.6 g/s of air at an air stoichiometry of 250%. These nominal conditions were selected to approximate the midpoint of the expected stack operating range.

Transfer functions from the resistive heater inputs to the system outlet temperatures were then derived and the sensitivity of the pole locations to disturbances in the total air mass flow rate was examined. Table 3 summarizes the open loop time constants and DC-gains ($\delta T_{g,\text{cv},o} / \delta Q_{\text{cv}}|_{s=0}$) for this range of air flow for each of the three systems. The total air mass flow rate range considered, $W_a = 0.3 - 0.9$ g/s, represents a humidification system disturbance for PEMFC stack electrical loads between 0.15–0.45 A/cm^2. The linear and nonlinear systems were compared, both to steps in heater inputs and air mass flow rates, indicating that the linear system response well approximates the nonlinear system for small deviations from nominal conditions.

Transfer functions can also be expressed from the air flow disturbance to the outlet temperatures. However, the DC-gains of these transfer functions indicate that there is a very small change in the steady-state heat required for a change in air mass flow rate. As a result, the use of static feedforward to reject air flow disturbances does not significantly improve temperature regulation. Therefore, only transfer functions from the heater inputs to the temperature outputs will be presented here.

The first order analytical transfer function from the bypass heater input to the bypass air outlet temperature, assuming the dry air mass flow rate is constant, is expressed as

$$\frac{\delta T_{a,\text{bp},o}}{\delta Q_{\text{bp}}} = \frac{b_{0,\text{bp}}}{s + p_{\text{bp}}} \tag{11}$$

where

$$b_{0,\text{bp}} = \frac{2}{m_{\text{bp}} C_{\text{bp}}}$$

Table 3 Open loop characteristics for $W_a = 0.3 - 0.9$ g/s

System	DC-gain (°C/W)	Time constant (s)
Water circulation	0.11–0.10	1562–1471
Bypass	6.93–3.32	123–59
Mixer	1.01–0.52	714–498

$$p_{\text{bp}} = \frac{2W^o_{a,\text{bp},i}C_{p,a} + \hbar^o_{b2\text{amb,bp}}A_{b2\text{amb,bp}}}{m_{\text{bp}}C_{\text{bp}}} \approx 0.013$$

The bypass pole location p_{bp} is a function of the air mass flow rate through the bypass, which will influence the system response time and DC-gain $\delta T_{a,\text{bp},o}/\delta Q_{\text{bp}}|_{s=0}$, as indicated in Table 3. An increased air mass flow rate causes an increase in the bypass pole location, resulting in a faster response time and smaller DC-gain. Qualitatively, a step in heat added to the bypass will increase the bypass temperature by a smaller amount at high air flow, as compared with low air flow; or alternatively, more energy is required to maintain the system temperature as air flow increases.

A transfer function from the water heater actuator input to the humidifier air outlet temperature is expressed as

$$\frac{\delta T_{g,\text{hm},o}}{\delta Q_{\text{hm}}} = \frac{b_0(s+z_1)}{(s+p_{l,\text{wh}})(s+p_{l,\text{hm}})(s+p_{a,\text{hm}})(s+p_{l,r})(s+p_{b,r})}, \tag{12}$$

where the coefficient in the numerator b_0 and the pole and zero locations can be analytically represented as functions of the heat transfer coefficients, the control volume masses, and specific heats. At the nominal conditions, $b_0=3.39\times10^{-6}$, the poles, and zero are located at $p_{a,\text{hm}}=1.23$, $p_{l,\text{hm}}=0.292$, $p_{l,r}=0.090$, $p_{b,r}=6.6\times10^{-4}$, $p_{l,\text{wh}}=0.014$, and $z_1=0.0094$, with a pole-zero cancellation between $z=p_{b,\text{wh}}=0.016$. The fastest control volume response time (pole location furthest from the origin on the complex s-plane) is associated with the humidifier air, followed by the liquid water volumes. The bulk material volumes have the slowest response time.

By varying the nominal air mass flow rate through the humidifier from $W_{a,\text{hm},i}=0.21-0.63$ g/s, the open loop time constant decreases from 1562 s to 1471 s, respectively. Thus, as with the bypass, the water circulation system response time increases for increasing air mass flow rates. This change in the time constants is most influenced by the slowest pole, which varies from a location on the real axis of the complex s-plane from $s=-0.0007$ to $s=-0.0009$ across the range of humidifier air mass flow rates considered. Note that, although the pole locations are significantly influenced by the liquid water mass flow rate, this variable is not a disturbance to the system and can be regulated at a fixed value throughout the experiments. As a result, the sensitivity of the pole locations to liquid water flow is not considered here.

The mixer thermal dynamics are described by a two state system, including the air-vapor mixture and the bulk materials. At the nominal conditions, the pole associated with the gas state is located at $s=-0.132$, while the pole associated with the bulk materials is located at $s=-0.0017$, indicating a significant bandwidth separation between these two states. As a result, assuming that $\delta T_{g,\text{mx},o}/dt=0$, which is a first order analytical transfer function from the mixer heater input to the gas outlet temperature, is expressed by

$$\frac{\delta T_{g,\text{mx},o}}{\delta Q_{\text{mx}}} = \frac{b_{0,\text{mx}}}{s+p_{\text{mx}}} \tag{13}$$

where

$$b_{0,\text{mx}} = \hbar^o_{b2g,\text{mx}}A_{b2g,\text{mx}}/\beta_{3,\text{mx}}$$

$$\beta_{1,\text{mx}} = \hbar_{b2\text{amb,mx}}A_{\text{mx}} + \hbar^o_{b2g,\text{mx}}A_{b2g,\text{mx}}$$

$$\beta_{2,\text{mx}} = (W^o_a C_{p,a} + W^o_{v,\text{hm},o}C_{p,v})$$

$$\beta_{3,\text{mx}} = m_{b,\text{mx}}C_{b,\text{mx}}(\beta_{2,\text{mx}} + \hbar^o_{b2g,\text{mx}}A_{b2g,\text{mx}})$$

$$p_{\text{mx}} = \frac{\beta_{1,\text{mx}}\beta_{2,\text{mx}} + \hbar_{b2\text{amb,mx}}A_{\text{mx}}\hbar^o_{b2g,\text{mx}}A_{b2g,\text{mx}}}{\beta_{3,\text{mx}}}$$

Comparing the nonlinear full order model to this linear reduced order model of the mixer thermal dynamics during step changes in the mixer heat shows an insignificant difference between the two dynamic models.

Clearly, the mixer pole location is a function of the air mass flow rate, either directly or indirectly through the heat transfer coefficient (between the bulk materials and the gases) or the water vapor mass flow rate. By varying the air mass flow rate from $W_a=0.3-0.9$ g/s, the pole location moves from $s=-0.0014$ to $s=-0.0020$, the time constant to a step in heat decreases from 714 s to 498 s, and the DC-gain decreases from 1.01°C/W to 0.52°C/W. As expected, by comparing the DC-gains of the bypass and mixer, more energy is required to raise the mixer temperature due to the larger air mass and the presence of water vapor in the mixer.

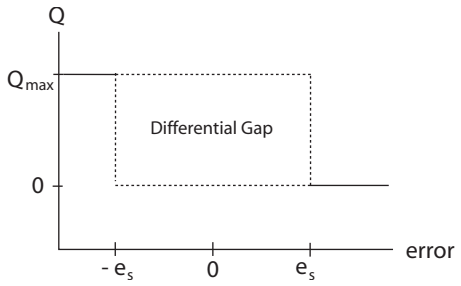

Fig. 3 Thermostatic control signal versus temperature error

5 Thermostatic Control

A simple and inexpensive control strategy for temperature regulation of a thermal system involves cycling a two position heater on or off at specified thresholds, as commonly implemented with thermostats. Thermostatic control is widely used for industrial automatic feedback systems due to its simplicity and cost effectiveness. A commonly recognized disadvantage to thermostatic control is the cycling of the actuator due to the repeated on-off action resulting from sensor noise. To reduce this cycling, hysteresis is often incorporated to construct a region about the desired temperature for which no control action takes place, known as the differential gap [11]. Figure 3 relates the error signal e to the control input Q for this thermostatic controller with hysteresis. Refer back to Figs. 1 and 2 for illustrations of the signal paths detailing the controllers and plants for the humidification feedback control system.

Temperature error dead bands establish the boundaries of the differential gap. When the temperature error $e=T^*-T$ is less than the lower error bound $e<-e_s$, the heater is on $Q=Q_{\max}$. When the temperature error is greater than the higher error bound $e>e_s$, the heater is off ($Q=0$). For errors within the error bounds, there is hysteresis, such that the heater is either on or off, depending upon the previous state of the heater. In this application, the resistive heater has been modeled as a nonideal relay, where the actuator "off" position is $Q=0$. For an ideal relay, the actuator off position would be $-Q_{\max}$. This is an important distinction, which will be discussed in more detail later. In summary, the discrete time thermostatic control law is represented by

$$u(k) = \begin{cases} Q_{\max} & \text{for} \quad e(k) \le -e_s \\ 0 & \text{for} \quad e_s \le e(k) \\ u(k-1) & \text{for} \quad -e_s < e(k) < e_s \end{cases} \tag{14}$$

Some degree of temperature overshoot $|e|>|e_s|$ is expected after the heater changes state; thus, the steady temperature response is oscillatory. The frequency and magnitude of these induced limit cycle oscillations depend on the system thermal dynamics and the error bounds e_s. The error bound will be selected to keep the error e within a specified limit cycle amplitude a.

Selecting this error bound e_s is not trivial. Both a describing function methodology, as well as a simulation based strategy, were

Table 4 Summary of thermostatic control results

System	Error bound (°C)	Amplitude (°C)	Period (s)
Bypass	0.38	0.5	2
Mixer	0.38	1.0	n/a
Water circulation	0.21	0.5	58

employed to tune the thermostatic controllers for the three resistive heaters. Table 4 summarizes the calculated amplitude and, where applicable, the temperature limit cycle period for each of the three regulated systems evaluated at the nominal conditions. The specific methodologies employed for each thermostatic controller to produce these results are detailed in the following subsections.

5.1 Water Circulation System Tuning With Describing Function Method. The behavior of a system nonlinearity, such as a relay, can be analytically evaluated by constructing a describing function that approximates the nonlinear response of the relay. Describing functions were used to quantify the amplitude and frequency of limit cycles induced in relay feedback systems [12,13], and subsequently used in the tuning of process controllers [14].

The describing function that approximates the behavior of a hysteretic relay nonlinearity was derived for a relay, which produces either a positive or negative output, such as $u=\pm Q_{\max}$, depending upon the state of the relay [15]. The physical heater actuators employed, however, do not allow negative heat to be added to the control volume, as shown by the on-off thermostatic control law specified in Eq. (14). As a result, the describing function in Ref. [15] was shifted and scaled (as shown in Fig. 4), to derive the describing function for a shifted relay with hysteresis

$$N(a^*,e_s)=\frac{Q_{\max}}{2}\left[\frac{4}{\pi a^*}\left(\sqrt{1-\left(\frac{e_s}{a^*}\right)^2}-j\frac{e_s}{a^*}\right)+1\right] \quad (15)$$

where a^* is the desired temperature limit cycle amplitude.

In a relay feedback system, the output temperature of the thermal process $\delta T(s)=G(s)\delta Q(s)$, where $G(s)$ denotes the plant transfer function (shown in Sec. 4.3), oscillates with a temperature amplitude of a and frequency ω. Assuming there is no change in the reference temperature and no disturbances to the system, the error bound e_s and the resulting frequency of oscillation ω can be determined for a given desired amplitude a^* by satisfying both the real and imaginary parts of $G(j\omega)N(a^*,e_s)=-1+0j$. Alternatively, a range of e_s values could be selected and the intersection of $G(j\omega)N(a^*,e_s)$ with the point $-1+0j$ could be found graphically. In general, as the differential gap expands, implying that e_s increases, the resulting limit cycle oscillation amplitude increases and the frequency decreases. If it is desired to specify the limit cycle oscillation frequency and amplitude, not just the amplitude, then an iterative process must be used since there is no guarantee that the selected amplitude and frequency pair will result in a feasible error bound.

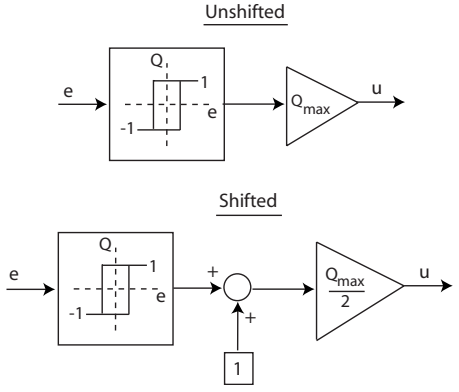

Fig. 4 Schematic comparing an unshifted versus a shifted relay with hysteresis

This methodology depends on the specification of the desired limit cycle oscillation. If this value is not known, the desired amplitude can be calculated by a combination of the smallest achievable output amplitude a_{ideal}, which occurs for an ideal relay with no hysteresis, and the standard deviation in the temperature signal at steady-state (temperature measurement noise) σ_n. The process used to select a desired amplitude involved the following steps.

(1) A describing function for a shifted ideal relay is formulated by setting $e_s=0$ in Eq. (15).
(2) The resulting output amplitude, which corresponds to the smallest achievable amplitude a_{ideal} is calculated by solving $G(j\omega)N(a^*=a_{\text{ideal}},e_s=0)=-1+0j$.
(3) The standard deviation in the measurement output noise σ_n is quantified.
(4) A combination of the smallest achievable output amplitude and the measurement noise is constructed, such as $a^*=a_{\text{ideal}}+3\sigma_n$.

For the type T thermocouples used to measure the system temperature, the standard deviation in the measurement noise is approximately $\sigma_n\approx 0.08\,^\circ$C. Using the ideal relay with no hysteresis and the plant transfer function given in Eq. (12) for the water circulation system, the smallest achievable humidifier air outlet temperature oscillations are $a_{\text{ideal,wh}}\approx 0.25\,^\circ$C. As a result, the smallest output amplitude for the water circulation system that makes the thermostatic controller least sensitive to noise is $a^*_{\text{wc}}\approx 0.5\,^\circ$C. From the evaluation of $(\delta T_{g,\text{hm},o}/\delta Q_{\text{wh}})\times(j\omega)N(a^*_{\text{wc}},e_{s,\text{wc}})=-1+0j$, the resulting error bound for the water heater is $e_{s,\text{wc}}\approx 0.2\,^\circ$C, which induces a limit cycle of frequency $\omega_{\text{wc}}\approx 0.11$ rad/s (corresponding to an oscillation period of 58 s) to maintain the desired output amplitude.

The ability of the describing function methodology to accurately estimate the temperature limit cycles was then evaluated by simulating the relay feedback system applied to the nonlinear water circulation system model, as shown in Fig. 5. The nonlinear model was evaluated at the nominal conditions, from Table 2, with no changes in the reference temperature. Generally, the describing function methodology resulted in the selection of error bounds, which induce a reasonably expected humidifier air outlet temperature limit cycle period at the desired amplitude.

The induced humidifier air outlet temperature limit cycle oscillates with a period of 77 s, which is larger than the 58 s expected. However, the nonlinear system response oscillates between the forced $u=\delta Q_{\max}$ and the free response $u=0$ when the actuator is turned on and off, resulting in different dynamic response times. Starting at the minimum humidifier air outlet temperature, it takes approximately 31 s to reach the maximum temperature, indicating an oscillation period of 62 s if the free response time were equal to the forced response time. Due to system nonlinearities and the difference between the free and forced dynamic plant responses, the temperature limit cycles are not symmetric about the reference value of $\delta T^*=0$; however, the desired limit cycle amplitude is achieved.

Varying the air mass flow rate supplied to the humidifier between $W_{a,\text{hm},i}=0.21-0.63$ g/s (a total air mass flow rate range of 0.3–0.9 g/s at $r_{\text{hm}}=0.7$), the required error bounds range from $e_s\approx 0.14-0.26\,^\circ$C to maintain the desired output amplitude of $a^*=0.5\,^\circ$C. This change in air mass flow rate also changes the period of oscillation ranging between 52 s and 74 s. In summary, the air mass flow rate does not significantly impact the necessary error bounds and resulting frequency of oscillation, to motivate the use of variable error bounds for the water circulation system.

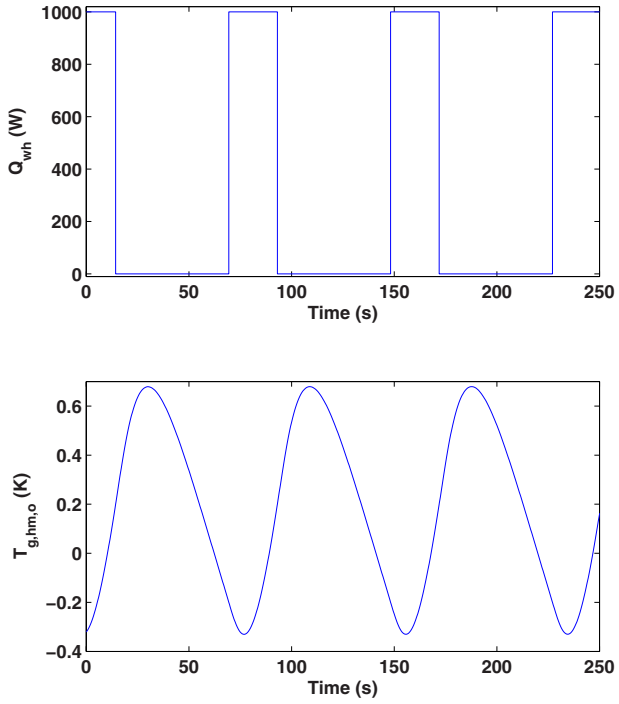

Fig. 5 Simulation of the temperature oscillations induced in the nonlinear water circulation system with relay feedback

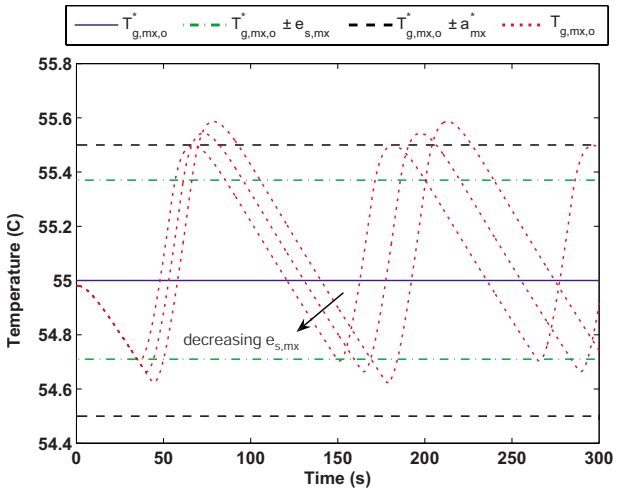

Fig. 6 Influence of the mixer error bound on the simulated nonlinear mixer outlet temperature limit cycle for a relay feedback system

5.2 Bypass and Mixer Tuning by Simulation. For first order plants, the describing function methodology cannot be employed to analytically calculate the thermostatic error bounds. The Nyquist plot of a first order plant remains in the right hand plane. Thus, no intersection exists between the describing function, which accounts for the fundamental component of the nonlinear relay element, and the plant Nyquist. Instead, simulations of the nonideal relay feedback system are used to examine the resulting temperature limit cycles for the bypass and mixer systems.

To tune the thermostatic error bounds using a simulation based approach, first, the error bound is set equal to the desired amplitude of the output temperature oscillations. The error bound is then incrementally reduced until the simulated temperature error is less than the desired amplitude. This process is summarized as follows.

(1) The desired output amplitude a^* is selected.
(2) The initial temperature error bounds are chosen to be equal to the desired temperature output amplitude, such that $e_s = a^*$.
(3) The closed loop nonideal relay feedback system response is simulated using the nonlinear plant model evaluated at the nominal operating conditions.
(4) The simulated temperature error signal is compared with the desired amplitude.
(5) If the simulated temperature error remains smaller than the desired amplitude throughout the simulation, then the search is terminated. Otherwise, the temperature error bounds are reduced and steps 3–5 are repeated.

To illustrate the iterative error bound tuning process and the relationship between the temperature limit cycle amplitude and period as a function of the error bound, consider the mixer system, assuming constant gas temperatures supplied from the humidifier and bypass (implies constant reference temperature), as shown in Fig. 6. As expected, as the error bound is decreased, both the period and amplitude of the temperature limit cycle decrease. When the error bound is reduced sufficiently that the induced temperature limit cycle amplitude a_{mx} is less than or equal to the desired amplitude a^*_{mx}, the iteration process is terminated and the necessary error bound has been identified.

Of course, in the physical system, the thermostatically controlled water heater will induce humidifier gas outlet temperature oscillations that influence both the bypass and the mixer, as inputs and/or dynamic reference temperatures. Therefore, it is recommended that the bypass and mixer thermostatic controllers be tuned in a manner that accounts for the water circulation system performance. By first selecting the water heater error bounds, as discussed in Sec. 5.1, the error bounds for the bypass relay feedback system can be determined using the simulation based iterative approach described above. Then, given the error bounds for the bypass and water heater, the error bounds for the mixer relay feedback system can be determined via simulation. This process of sequential controller tuning is described schematically in Fig. 7.

In selecting the desired amplitudes for the bypass and mixer, consideration of the system dynamics must be made. The water circulation system (humidifier) response influences both the mixer and bypass by establishing an oscillating reference temperature. As with the water heater, to reduce heater relay cycling due to measurement noise, the desired bypass temperature limit cycle amplitude was selected to be $a^*_{bp}=0.5\,^\circ$C. However, the water circulation system, does not only influence the mixer through the reference temperature. The mixer also receives air and water vapor from the humidifier. As a result, oscillations in the humidifier will cause oscillations in the mixer, even when the mixer heater is off. As a result, the mixer amplitude was selected to be $a^*_{mx}=1.0\,^\circ$C to account for the $0.5\,^\circ$C amplitude fluctuations due to the water circulation system.

Applying this iterative and sequential simulation based tuning approach, at the nominal operating conditions, the bypass error bound was found to be $e_{s,bp}=0.38\,^\circ$C to achieve a temperature limit cycle amplitude of $a^*_{bp}=0.5\,^\circ$C and the mixer error bound was $e_{s,mx}=0.38\,^\circ$C to achieve a temperature limit cycle amplitude of $a^*_{bp}=1.0\,^\circ$C. Although the error bounds for the bypass and mixer are the same, the two systems achieve very different temperature limit cycle amplitudes due to the relatively slow thermal response of the mixer, as compared with the bypass.

The influence of the total air mass flow rate on the mixer and bypass error bounds was considered by identifying the respective error bounds at different flow rates. As with the water circulation system, a range of total air mass flow rates between 0.3 g/s and 0.9 g/s was considered, assuming 70% of the air is delivered to the

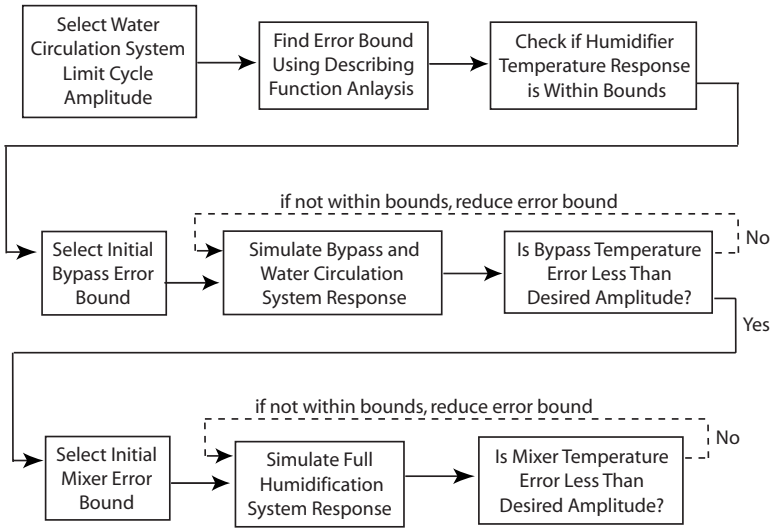

Fig. 7 Sequential process used to tune the bypass and mixer thermostatic error bounds

humidifier ($r_{hm}=0.7$). The bypass error bounds show little sensitivity to the air mass flow rate, ranging from $e_{s,bp}=0.36-0.41\,^{\circ}C$. Of course, if low relative humidity operation is desired, more air would be supplied to the bypass, resulting in a greater sensitivity in the bypass error bounds. The mixer error bounds, however, exhibit a greater degree of sensitivity to the total air mass flow rate, ranging from $e_{s,mx}=0.14-0.65\,^{\circ}C$ to achieve the desired temperature limit cycle amplitude of a^*_{mx}. As the total air mass flow rate increases, the necessary mixer error bounds increase. Such sensitivity to the total air mass flow rate could motivate the use of variable mixer error bounds. However, constant error bounds could still be used with the understanding that the desired amplitude will only be achieved at the total air mass flow rate that the controller was tuned for.

6 Proportional Integral Control

The thermostatic controllers, designed in Sec. 5, are inexpensive to implement and are capable of regulating temperature to within $1\,^{\circ}C$ of the desired cathode inlet temperature. If, however, zero steady-state temperature error is required or the limit cycle temperature oscillations are undesirable, a more sophisticated controller is needed. With the addition of controller integrator states, zero steady-state error to a step command in the reference temperature can be achieved. As a result, proportional integral (PI) control was considered due to the simplicity of tuning with time domain constraints and guarantee of zero steady-state error. Note, however, that in contrast to thermostatic control, PI control requires the heater actuators to be capable of producing a variable heat transfer rate. Thus, there is a tradeoff between regulation capability and hardware and software complexity.

The PI controller is expressed in the frequency domain as

$$\delta Q = \left(k_{P,cv} + \frac{k_{I,cv}}{s}\right)e \tag{16}$$

where the proportional and integral controller gains are denoted by $k_{P,cv}$ and $k_{I,cv}$, respectively, for each control volume. By substitution into Eqs. (11) and (13), the mixer and bypass closed loop transfer functions from the reference to the actual temperature is described by

$$\frac{\delta T_{g,cv,o}}{\delta T^*} = \frac{b_{o,cv}k_{P,cv}(s+k_{I,cv}/k_{P,cv})}{s^2+(b_{o,cv}k_{P,bp}+p_{cv})s+b_{o,cv}k_{I,bp}} \tag{17}$$

where p_{cv} is the open loop pole location. The PI controller gains can be tuned upon inspection of the characteristic polynomial of this closed loop transfer function. For tuning the controller gains, two of the following three time domain constraints are selected: from (1) the proportional controller gain; (2) response time; and (3) the damping coefficient (overshoot).

The mixer and bypass proportional gains are selected based on the expected maximal actuator heater power (at steady-state over the range of operating conditions) supplied $Q_{design,cv}$ for a specified temperature error $e_{design,cv}$, such that

$$k_{P,cv} = \frac{Q_{design,cv}}{e_{design,cv}} \tag{18}$$

Given an expected error of $e_{design,cv}=1.0$ K (corresponding to $a^*=0.5$ K used for thermostatic controller tuning) and the maximum steady-state heater power of $Q_{design,bp}=15$ W and $Q_{design,mx}=25$ W, the proportional gains are $k_{P,bp}=15$ W/K, $k_{P,mx}=25$ W/K. For a critically damped response, the resulting integral controller gains can then be calculated.

The closed loop transfer function from the desired humidifier air outlet temperature to the actual temperature is of the sixth order; therefore, time domain design constraints (overshoot, settling time, etc.) cannot be used analytically to specify the controller gains. Instead, iterative pole placement was used to achieve a desired closed loop response. From inspection of the open loop water circulation system poles and zeros, a stable slow pole is located on the real axis at approximately $s=-0.0008$. This pole could be shifted or canceled by a carefully tuned PI controller. Because the humidifier water circulation system has an air flow input disturbance and the model parameters were well identified, a pole shifting controller was employed for improved input disturbance rejection [16]. Using the linearized model of the water circulation system shown in Eq. (12), the PI controller was tuned to achieve a fast response with less than 20% overshoot.

A summary of the final controller gains and resulting settling times to a step in the reference temperature is shown in Table 5, along with the gain and phase margins. To prevent integrator windup, a logic based case structure was employed, which enables or disables the integrator while the actuator is saturated at $Q_{cv}(t)=0$ or $Q_{cv}(t)=Q_{max,cv}$.

7 Experimental Controller Comparison

The closed loop thermostatic and PI controller experimental responses, for a step in the cathode inlet reference temperature from nominal conditions, is shown in Figs. 8–11. As expected, the system response with thermostatic feedback regulation results in

Table 5 Proportional-integral controller gains and system response

Heater	$k_{P,cv}$	$k_{I,cv}$	t_{settle} (s)	GM (dB)	PM (deg)
Bypass	15	3.25	9.4	∞	142
Mixer	25	0.22	256	∞	145
Water heater	263	1.60	176	20	138

temperature and humidity limit cycles, while PI feedback control enables reference tracking with zero steady-state error.

Using thermostatic control, the desired humidifier air outlet temperature limit cycle amplitude of $a^*_{wc}=0.5\,^\circ$C was achieved, see Fig. 8, as was the oscillation period. The time required to transition from the minimum to maximum humidifier air outlet limit cycle temperature is approximately 34 s, corresponding to a 68 s oscillation period if the free and forced response times were the same, agreeing with the simulation results. For the water circulation system PI controller, the resulting overshoot following the step in the reference temperature is larger than predicted in simulation, but still within the designed 20%.

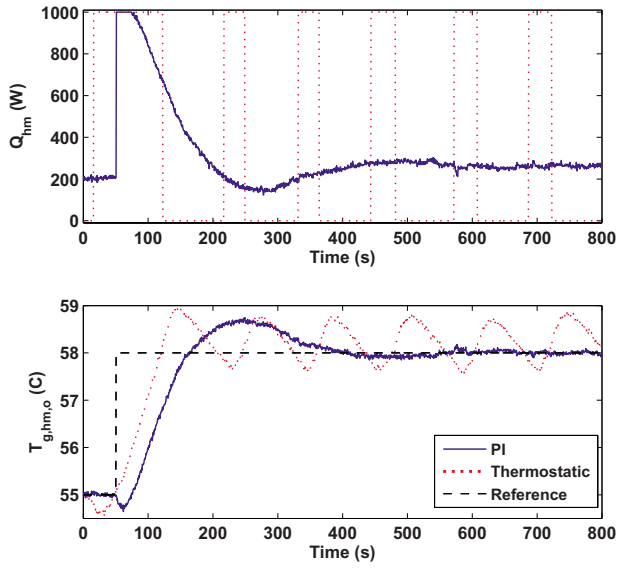

Fig. 8 Experimental humidifier air outlet closed loop temperature response to a reference step, comparing PI and thermostatic control

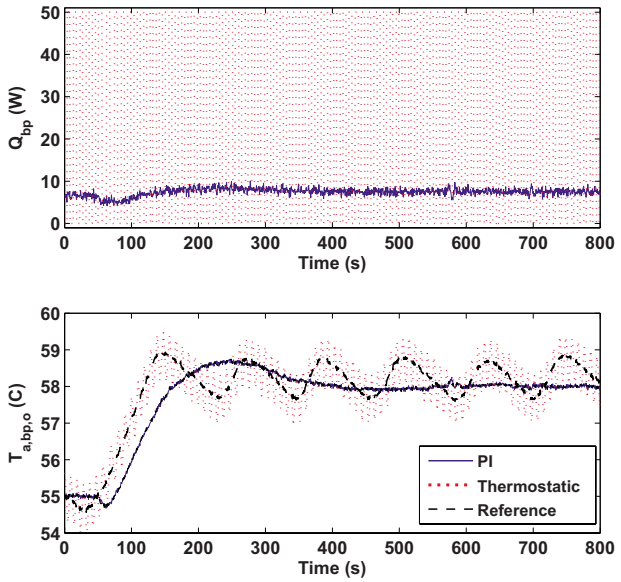

Fig. 9 Experimental bypass air outlet closed loop temperature response to a reference step, comparing PI and thermostatic control

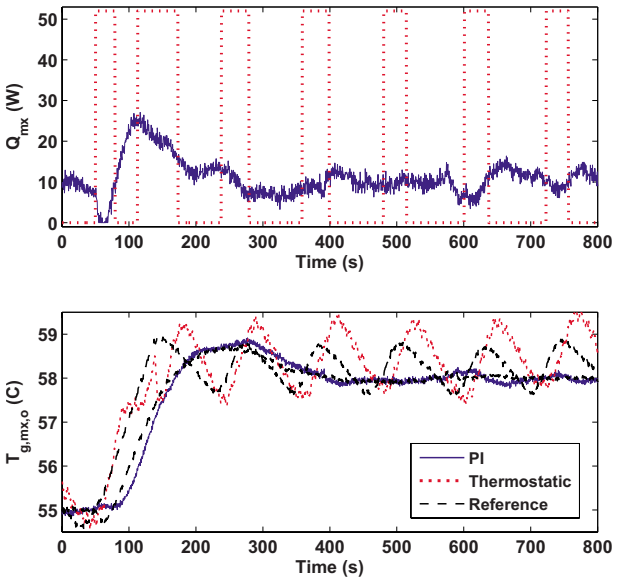

Fig. 10 Experimental mixer air outlet closed loop temperature response to a reference step, comparing PI and thermostatic control

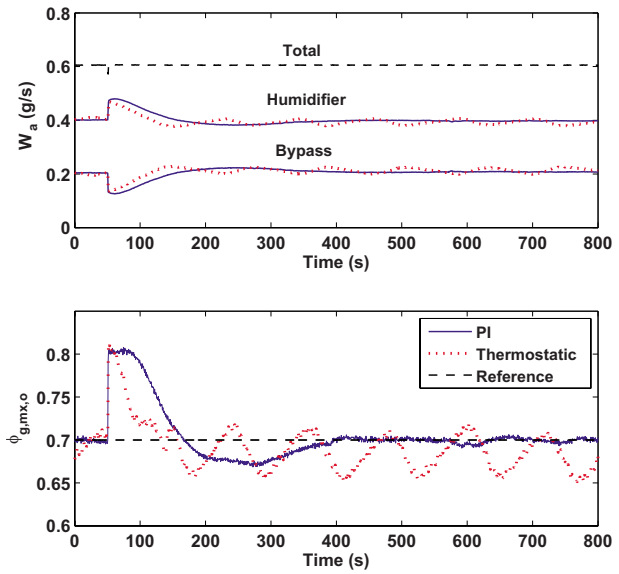

Fig. 11 Mixer gas outlet relative humidity response to a step in the reference temperature, comparing PI and thermostatic control

The experimental response of the closed loop bypass system to this step in the reference cathode inlet air temperature is shown in Fig. 9, comparing thermostatic and PI controls. The resulting temperature limit cycle amplitude is approximately 0.5°C, as designed. Throughout the experiment, the PI controller is capable of tracking the dynamic reference humidifier air outlet temperature with approximately zero steady-state error.

The experimental response of the closed loop mixer system to this step in the reference cathode inlet air temperature is shown in Fig. 10, comparing thermostatic and PI controls. The limit cycle amplitude was found to be slightly less than the designed 1°C. The mixer PI controller performed as expected throughout the experiment.

The experimental mixer air outlet relative humidity response for this temperature reference step is shown in Fig. 11. Because the actual mixer outlet temperature response is approximately sinusoidal using thermostatic control, the relative humidity also exhibits an approximately sinusoidal response. Both in simulation and in the experiment, the maximum excursion in the mixer air outlet relative humidity is approximately 10% for both controllers. Note that the mixer gas outlet relative humidity presented here is an estimation based on physical measurements applying Eq. (7).

8 PI Closed Loop Disturbance Response

Using the feedforward control of the air mass flow rate and proportional integral control of the resistive heaters, another closed loop experiment was conducted for changes in the system references (cathode inlet temperature and relative humidity) and the system disturbances (ambient temperature, total air mass flow, and a reservoir fill event). As expected, the PI controller results in zero steady-state error. The overshoot and response time, following step changes in the reference temperature, is approximately equal to the response that the controller was tuned to achieve.

Figure 12 shows the humidifier air outlet temperature response to disturbances. Interestingly, the cathode inlet reference temperature step results in an increase in the air flow supplied to the humidifier, causing an initial decrease in the humidifier air outlet temperature, which resembles a nonminimum phase response, but is actually due to the feedforward regulation of the air flow. The rapid 10°C increase in ambient temperature increased the humidifier air outlet temperature, requiring the humidifier heater power to decrease to regulate the air temperature. A decrease in total air flow resulted in a decrease in the fraction air supplied to the humidifier, in turn, increasing the humidifier air outlet temperature. The reservoir fill event, which injects cold water into the reservoir, causes a dramatic decrease in the humidifier air outlet temperature that initially saturates the water heater. Finally, the decrease in desired cathode inlet relative humidity decreases the humidifier air flow, in turn, increasing the air outlet temperature.

The response of the bypass system to these disturbances is shown in Fig. 13. Again, the intent of the bypass controller is to track the humidifier air outlet temperature. The bypass adequately tracks the humidifier air outlet temperature excursions well, due to the difference in closed loop response times of these two systems. There is an insignificant difference between the bypass and humidifier air outlet temperatures throughout the experiment.

When the humidifier air outlet temperature initially decreases, following the increase in the cathode inlet temperature reference, the mixer heater turns off and then proceeds to track the humidifier air outlet temperature, as shown in Fig. 14. In general, the ability of the mixer to track the humidifier is adequate. Additionally, the mixer outlet relative humidity is well regulated throughout the experiment. Although the relative humidity at the mixer outlet was relatively well regulated with thermostatic control, the temperature oscillations may not be desirable, depending upon the operating conditions of the PEMFC stack to which the air is supplied. To eliminate these oscillations, the PI controller is recommended to guarantee zero steady-state temperature error. The

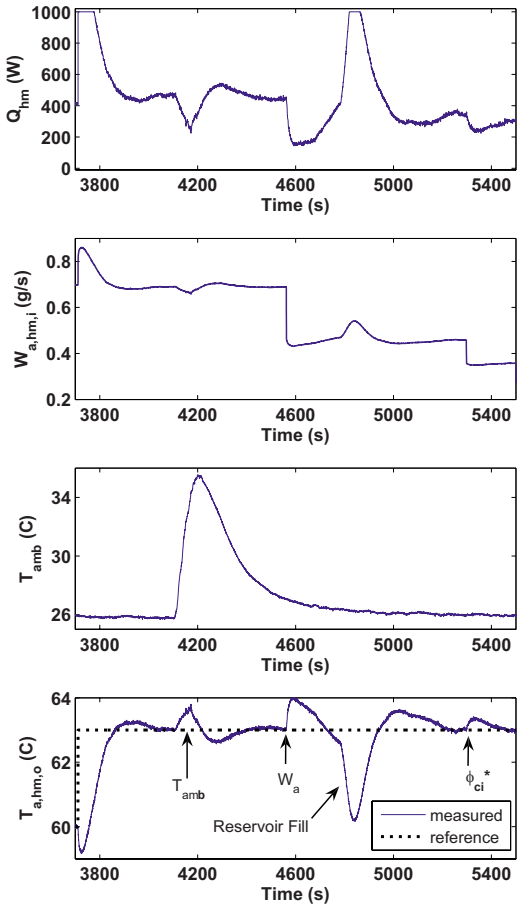

Fig. 12 Humidifier air outlet temperature response to disturbances using PI control

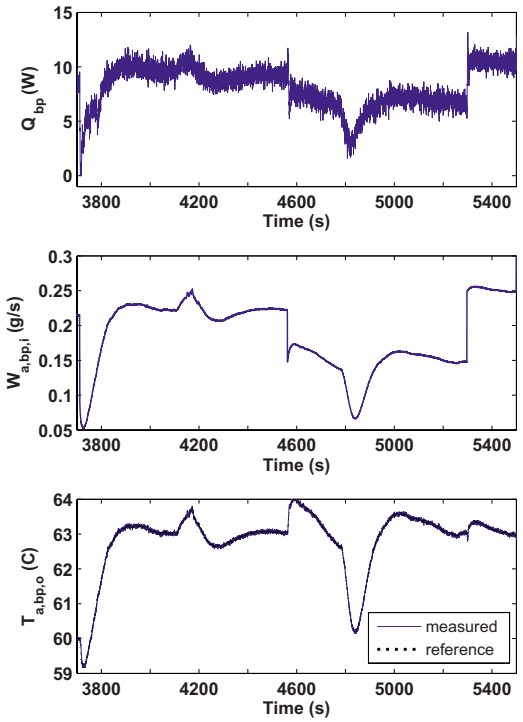

Fig. 13 Bypass air outlet response to disturbances using PI control

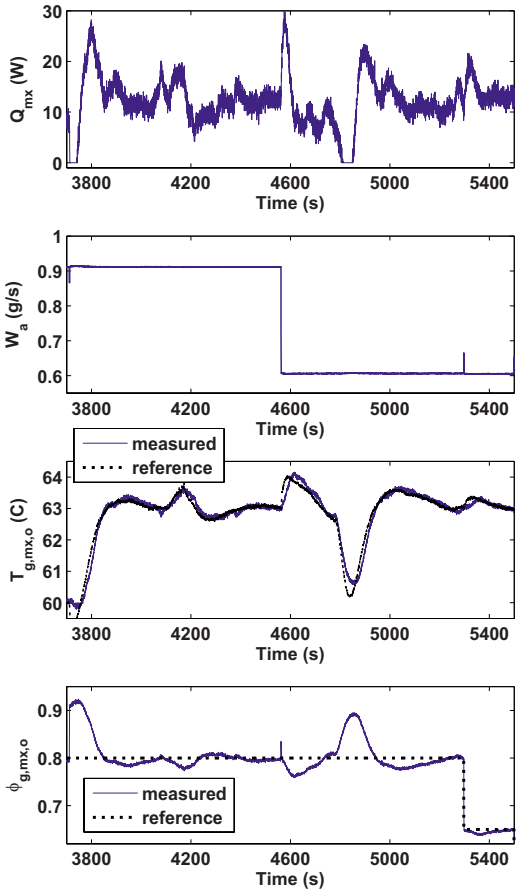

Fig. 14 Mixer outlet response to disturbances using PI control

added hardware complexity of a variable heater, in light of the potentially slower response time for small temperature changes, may not justify the use of PI control. If variable heaters are available with no cost or reliability penalty with respect to control implementation, then the PI controllers are recommended.

9 Conclusions

An experimentally validated model of the humidification system thermal dynamics was employed to design and tune controllers for thermal and humidity regulation. Thermostatic and proportional integral controllers were considered for thermal regulation, and a static nonlinear feedforward map was employed to control the air split between the humidifier and bypass. For constant disturbances, the humidification system dynamics are approximately linear, enabling the linear control theory to be applied for controller tuning. As expected, thermostatic control of the humidification system, tuned using either a describing function or simulation based methodology, resulted in temperature and relative humidity limit cycle oscillations. PI control, however, allowed for adequate control of both temperature and humidity with zero steady-state temperature error, while satisfactorily minimizing excursions in temperature, following changes in the disturbances. Therefore, a tradeoff exists between steady-state thermal regulation, hardware, and controller simplicity, which is a critical consideration for automotive applications.

Acknowledgment

Funding is provided by the U.S. Army Center of Excellence for Automotive Research (Grant No. DAAE07-98-3-0022) and the National Science Foundation (Grant No. CMS 0625610).

Nomenclature

Variables

A = surface area available for heat transfer (m^2)
C_p = constant pressure specific heat (J/kg K)
C = constant volume specific heat (J/kg K)
$\hbar$ = heat transfer coefficient (W/m^2 K)
h = specific enthalpy (J/kg)
m = mass (kg)
M = molecular weight (kg/mol)
p = pressure (Pa) or pole location
Q = heat added to a control volume (W)
r = mass flow ratio, fraction of total flow
t = time (s)
T = temperature (K)
W = mass flow rate (kg/s)
β = heat transfer coefficient parameters
δ = deviations from nominal conditions
ϕ = relative humidity (0–1)
ω = humidity ratio

Subscript and Superscript Symbols

a = air
amb = ambient
bp = bypass
b = control volume bulk materials
ca = fuel cell cathode
cv = control volume
fc = fuel cell stack
g = gas constituent
hm = humidifier
i = into the control volume
l = liquid water
mx = mixer
o, out = out of the control volume(subscript), nominal value (superscript)
r = reservoir
sat = saturation
v = water vapor
wc = water circulation system (humidifier, reservoir and water heater)
wh = water heater
* = desired value

References

[1] Varigonda, S., and Kamat, M., 2006, "Control of Stationary and Transportation Fuel Cell Systems: Progress and Opportunities," Comput. Chem. Eng., **30**, pp. 1735–1748.
[2] McKay, D., Siegel, J., Ott, W., and Stefanopoulou, A., 2008, "Parameterization and Denise McKay FC-09-1080 40 Prediction of Temporal Fuel Cell Voltage Behavior During Flooding and Drying Conditions," J. Power Sources, **178**(1), pp. 207–222.
[3] Karnik, A., Stefanopoulou, A., and Sun, J., 2007, "Water Equilibria and Management Using a Two-Volume Model of a Polymer Electrolyte Fuel Cell," J. Power Sources, **164**, pp. 590–605.
[4] Love, A., Middleman, S., and Hochberg, A., 1993, "The Dynamics of Bubblers as Vapor Delivery Systems," J. Cryst. Growth, **129**, pp. 119–133.
[5] Choi, K., Park, D., Rho, Y., Kho, Y., and Lee, T., 1998, "A Study of the Internal Humidification of an Integrated PEMFC Stack," J. Power Sources, **74**, pp. 146–150.
[6] Staschewski, D., 1996, "Internal Humidifying of PEM Fuel Cells," Int. J. Hydrogen Energy, **21**(5), pp. 381–385.
[7] McKay, D. A., Stefanopoulou, A. G., and Cook, J., 2010, "A Controllable Membrane-Type Humidifier for Fuel Cell Applications—Part I: Operation, Modeling and Experimental Validation," ASME J. Fuel Cell Sci. Technol., **7**(5), p. 051006.
[8] Wheat, W., Clingerman, B., and Hortop, M., 2005, "Electronic By-Pass Control of Gas Around the Humidifier to the Fuel Cell," U.S. Patent No. 6,884,534.
[9] Cortona, E., Onder, C., and Guzzella, L., 2002, "Engine Thermomanagement With Electrical Components for fuel consumption reduction," Int. J. Engine Res., **3**(3), pp. 157–170.
[10] Setlur, P., Wagner, J., Dawson, D., and Marotta, E., 2005, "An Advanced Engine Thermal Management System: Nonlinear Control and Test," IEEE/

ASME Trans. Mechatron., **10**(2), pp. 210–220.
[11] Ogata, K., 1998, *System Dynamics*, Prentice-Hall, Englewood Cliffs, NJ.
[12] Khalil, H., 2002, *Nonlinear Systems*, Prentice-Hall, Englewood Cliffs, NJ.
[13] Slotine, J.-J., and Li, W., 1991, *Applied Nonlinear Control*, Prentice-Hall, Englewood Cliffs, NJ.
[14] Hang, C., Astrom, K., and Wang, Q., 2002, "Relay Feedback Auto-Tuning of Process Controllers—A Tutorial Review," J. Process Control, **12**(1), pp. 143–162.
[15] Taylor, J., 1999, "Describing Functions," *Electrical Engineering Encyclopedia*, Wiley, New York.
[16] Middleton, R., and Graebe, S., 1999, "Slow Stable Open-Loop Poles: To Cancel or Not to Cancel," Automatica, **35**, pp. 877–886.